Materials Research Letters

ISSN: 2166-3831 (Online) Journal homepage: www.tandfonline.com/journals/tmrl20

Impact of ε-martensite on the fracture resistance of high-Mn steels[1]

Qingquan Lai, Shuai Chang, Yuntao Wei, Shangshu Wu, Pascal Jacques, Thomas Pardoen & Guohua Fan

To cite this article: Qingquan Lai, Shuai Chang, Yuntao Wei, Shangshu Wu, Pascal Jacques, Thomas Pardoen & Guohua Fan (2024) Impact of ε-martensite on the fracture resistance of high-Mn steels[1], Materials Research Letters, 12:10, 700-708, DOI: 10.1080/21663831.2024.2372082

To link to this article: https://doi.org/10.1080/21663831.2024.2372082

© 2024 The Author(s). Published by Informa UK Limited, trading as Taylor & Francis Group.

View supplementary material

Published online: 21 Jul 2024.

Submit your article to this journal

Article views: 1620

View related articles

View Crossmark data

Citing articles: 7 View citing articles

Full Terms & Conditions of access and use can be found at
https://www.tandfonline.com/action/journalInformation?journalCode=tmrl20

MATER. RES. LETT.
2024, VOL. 12, NO. 10, 700–708
https://doi.org/10.1080/21663831.2024.2372082

MATERIALS RESEARCH LETTERS
Taylor & Francis
Taylor & Francis Group

ORIGINAL REPORTS

OPEN ACCESS
Check for updates

Impact of ε-martensite on the fracture resistance of high-Mn steels[1]

Qingquan Lai[1]*, Shuai Chang[2], Yuntao Wei[2], Shangshu Wu[1], Pascal Jacques[3], Thomas Pardoen[3] and Guohua Fan[1]*

[1]Key Laboratory for Light-Weight Materials, Nanjing Tech University, Nanjing, People's Republic of China; [2]Herbert Gleiter Institute of Nanoscience, Nanjing University of Science and Technology, Nanjing, People's Republic of China; [3]Institute of Mechanics, Materials and Civil Engineering, UCLouvain, Louvain-la-Neuve, Belgium

ABSTRACT

The formation of ε-martensite is generally considered as detrimental to cracking resistance. The essential work of fracture (EWF) of high-Mn steels with ε-martensite has been determined in the near plane-stress regime. The analysis of the thickness dependence of EWF shows that an alloy with more ε-martensite involves a higher work of material separation and a lower contribution from crack-tip necking. Therefore, the presence of ε-martensite leads to a lower cracking resistance at large thickness, but to an enhanced fracture toughness at small thickness. The beneficial effect of ε-martensite to the work of fracture is explained by an increased strength without any reduction of void spacing, and related to the ε-martensite/austenite plastic co-deformation and to microcrack blunting and crack branching. The key finding of the study is thus that the best compromise depends on the structural application which imposes the strength and stiffness requirements, hence the thickness.

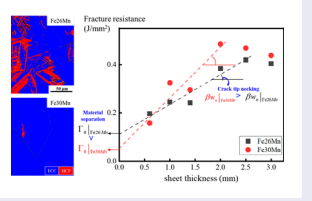

ARTICLE HISTORY
Received 10 May 2024

KEYWORDS
High-Mn steels; microstructure; martensite; fracture mechanisms; fracture toughness

Impact statement

- High-Mn steel with a larger amount of ε-martensite dissipates more energy in the fracture process zone, presenting superior fracture resistance at small thickness.
- Optimization of the mechanical performance depends on thickness.

Introduction

High-strength metallic materials are highly demanded in a wide range of modern technologies. But a high-strength material must be combined to adequate resistance to failure, including plastic localization and fracture, in order to fulfill the requirements for successful forming and structural operations. High-Mn steels [1–4] are promising structural materials owing to both high strength and large tensile ductility. In these alloys, the formation of ε-martensite is triggered during deformation due to the low stacking fault energy (SFE), leading to an enhanced strain hardening behavior. However, the ε-martensite has a hexagonal-close-packed (HCP) crystal structure, which is usually considered as a brittle phase, and the unwanted formation of this phase tends to deteriorate the ductility and fracture resistance [5–9].

Conventional uniaxial tensile testing provides information about the fracture strain under a low constraint on plastic deformation, involving the development of necking and damage evolution inside the neck. But for the pre-cracked specimens as used in fracture mechanics testing to represent cracked components, a higher stress triaxiality level with large associated maximum principal stress modifies the competition between plasticity and fracture, and can even change the dominant

CONTACT Qingquan Lai lai@njtech.edu.cn Key Laboratory for Light-Weight Materials, Nanjing Tech University, Nanjing 211816, China; Thomas Pardoen thomas.pardoen@uclouvain.be Institute of Mechanics, Materials and Civil Engineering, UCLouvain, 1348 Louvain-la-Neuve, Belgium
*Present address: Materials Academy, JITRI, Suzhou, People's Republic of China

Supplemental data for this article can be accessed online at https://doi.org/10.1080/21663831.2024.2372082.

© 2024 The Author(s). Published by Informa UK Limited, trading as Taylor & Francis Group.
This is an Open Access article distributed under the terms of the Creative Commons Attribution License (http://creativecommons.org/licenses/by/4.0/), which permits unrestricted use, distribution, and reproduction in any medium, provided the original work is properly cited. The terms on which this article has been published allow the posting of the Accepted Manuscript in a repository by the author(s) or with their consent.

damage mechanism [10,11]. The crack extension resistance is controlled by the localized damage evolution within the fracture process zone (FPZ) in the near crack tip region. Therefore, the fracture resistance can sometimes be ranked differently when using different test configurations and protocols [12–14], which sets significant challenges not only for the assessment of fracture resistance but also for a proper understanding of the key factors dictating the failure mechanisms.

This study is dedicated to unravel the effects of ε-martensite on the fracture resistance of high-Mn steels. The thin sheet format (typically < 3 mm) has technological relevance for a number of applications (e.g. car body manufacturing). Thin sheets, if sufficiently tough, fail under near plane stress conditions. Two kinds of energy contributions play a role during crack extension and impact the overall cracking resistance, that is, the work for material separation, including the damage accumulation, in the FPZ (Γ_0) and the crack tip necking energy (Γ_n) [15]. Therefore, the question is how the presence of ε-martensite influences these two energy terms? On the one hand, the formation of ε-martensite could accelerate the damage processes [6,16]. On the other hand, the ε-martensite formation is known to enhance the strain hardening and could contribute positively to the energy dissipation of crack tip necking [17–19]. The Essential Work of Fracture (EWF) method is appropriate to evaluate the fracture resistance of ductile thin sheets [20,21]. Recent progress has shown that based on the thickness dependence of EWF, the energy associated with material separation and crack tip necking can be elegantly partitioned [15,17,22,23]. Applying the EWF concept to clarify the influence of ε-martensite will provide a critical basis for engineering the formation of ε-martensite in relevant materials and give new insight about the optimization between strength and fracture resistance.

Materials and methods

The Fe–26wt.% Mn and Fe–30wt.%Mn binary alloys are selected as model materials for high-Mn steels involving ε-martensite formation. The α'-martensite phase is not formed in FeMn alloys with this range of composition [24,25]. The difference in Mn content leads to a different SFE (31.7 mJ/m^2 for Fe26Mn and 38.1 mJ/m^2 for Fe30Mn [26,27]) and thus to a change of the austenite stability and of the kinetics of ε-martensitic transformation during plastic deformation. The as-received Fe26Mn and Fe30Mn alloys were hot forged and annealed. After grinding and polishing, the metallographic preparation was followed by colloidal silica polishing and ion-beam treatment (details seen in [28]). The microstructures were characterized by scanning electron microscopy (SEM) equipped with an electron backscatter diffraction (EBSD) detector.

Uniaxial tensile tests were performed on dog-bone specimens designed according to ASTM E8 standard with a gauge section of 6 mm width, 2 mm thickness and 32 mm length, and at an engineering strain rate of 10^{-3}/s. The strain was determined using optical extensometry. The fracture strain of the broken uniaxial tensile specimens is defined as

$$\varepsilon_f = \ln \frac{A_0}{A_c}, \tag{1}$$

where A_0 is the initial cross-section area and A_c is the fracture surface area. The corresponding fracture stress (σ_f) is determined by dividing the load at fracture by A_c. The work of fracture under uniaxial tension (W_f^{uni}) [29] is approximated by

$$W_f^{uni} = \frac{1}{2}(\sigma_y + \sigma_u)\varepsilon_u + \frac{1}{2}(\sigma_y + \sigma_f)(\varepsilon_f - \varepsilon_u), \tag{2}$$

where σ_y, σ_u are the yield strength and true tensile strength, respectively, ε_u is true uniform elongation, σ_f and ε_f are the fracture stress and fracture strain as defined above. In addition, loading-unloading-reloading (LUR) experiments were also conducted on the uniaxial tension specimen in order to assess the magnitude of the back stress, following the procedure in Ref. [30].

The double-edge-notched tension (DENT) geometry is generally used for EWF measurements. The DENT specimens are 155 mm long and 45 mm wide. The initial ligament length (l_0) was varied from 6 to 12 mm and the initial thickness (t_0) was ranged from 0.6 mm to 3 mm. Notches with an initial opening of 250–300 µm were produced by electrical discharge machining. In order to ensure an initial crack tip smaller than the critical opening as verified after testing [20], the crack tip sharpening was induced with a fresh razor blade, leading to a crack tip radius between 50 and 100 µm. The DENT specimens were deformed at a crosshead speed of 0.3 mm/min, and the displacement was measured by a mechanical extensometer. The integration of the load-displacement response provides the total work of fracture W_f^{DENT}, and the specific fracture work (w_f) is calculated as

$$w_f = \frac{W_f^{DENT}}{l_0 t_0} = w_e + \alpha l_0 w_p, \tag{3}$$

where l_0 and t_0 are the initial ligament length and thickness, respectively, α is the shape factor of the diffuse plastic zone and w_p is the specific diffuse plastic work, w_e is the specific EWF [20]. A linear regression on w_f as a function of l_0 allows the separation of w_e and αw_p. The

energy expenditure in terms of materials separation (Γ_0) and crack tip necking (Γ_n) can be partitioned according to the following relationship [17,23]:

$$w_e = \Gamma_0 + \Gamma_n = \Gamma_0 + \beta w_n t_0, \tag{4}$$

where Γ_0 is the thickness independent part of w_e, w_n is an average work of necking per unit volume and β is a shape factor of the necking zone.

Results

Figure 1(a) and (b) show the microstructures of Fe26Mn and Fe30Mn. The volume fraction of ε-martensite in Fe26Mn is equal to 26 vol.%. The sequential formation of ε-martensite plates with different orientations divides the prior austenite grains, with microstructural characteristics being consistent with the literature [25]. The Fe30Mn exhibits a single-phase austenitic microstructure, which can also be justified by the Schumann diagram [24]. The residual martensitic islands in Figure 1(b) are presumably induced by mechanical polishing, and were not completely removed by ion milling from the polished surface (See Supplementary Figure S1).

Figure 1(c) presents the results of the uniaxial tensile tests. The higher initial ε-martensite fraction and the occurrence of transformation-induced plasticity (TRIP) in Fe26Mn favors the development of an heterodeformation-induced back stress [31,32], which increases both the yield strength and strain hardening rate, resulting in a higher flow stress compared to Fe30Mn. In Fe30Mn, the higher SFE leads to plastic deformation dominated by dislocation glide, and ε-martensite only forms after the onset of necking [25]. The difference in deformation heterogeneity is revealed by the LUR experiments as shown in Figure 1(d) and (e). Both Fe26Mn and Fe30Mn exhibit an hysteresis during the unloading and reloading cycle. But the magnitude of the hysteresis and back stress of Fe26Mn are much higher than that of Fe30Mn.

The damage is accelerated by the enhanced formation of ε-martensite in Fe26Mn, which explains the limited post-necking deformation ($\varepsilon_f - \varepsilon_u \sim 0.18$). The high ductility of Fe30Mn is characterized by a significant post-necking deformation ($\varepsilon_f - \varepsilon_u \sim 0.78$). Therefore, the strengthening induced by the ε-martensite compromises the fracture strain and toughness W_f^{uni} (Figure 1(f) and (g)), the trend being also found in other high-Mn steels [6,8,33,34]. This could be attributed to the insufficient number of independent slip systems of the HCP ε-martensite [35], and also to the high density of ε-martensite/ε-martensite and ε-martensite/grain boundary intersections, which generate a high density of damage nucleation sites [5,6,16]. Here in Figure 1, the response of a ferrite-martensite dual-phase steel with 36 vol. % α'-martensite (DP-36%) is taken from [23] for comparison. The DP-36% presents the best mechanical performance under uniaxial tension with respect to the balance of strength σ_y—fracture strain ε_f (Figure 1(f)) and strength σ_y—toughness in term of W_f^{uni} (Figure 1(g)) among the three steels.

The results of the EWF measurements are given in Figure 2. The load-displacement curves in Figure 2(a) and (b) show that the DENT specimens of both alloys are deforming plastically well before cracking initiation, involving a large crack tip opening displacement. The normalized load-displacement curves overlap for each alloy (Figure S2), and the peak load normalized by the initial ligament area does not vary with t_0 (Figure S3), which supports the validity of the EWF procedure according to [36,37]. The quality of the measurements is also substantiated by the satisfactory linear regression on the w_f–t_0 data (Figure S4). The details of the linear regression are summarized in Table 1.

Figure 2(c) compares the thickness dependence of w_e for the different steels. The values of w_e of DP-36% taken from [23] decrease monotonically with decreasing thickness. However, for Fe26Mn, w_e first increases more or less linearly with t_0 up to $t_0 = 2.5$ mm, and then reaches a peak at $t_0 = 2.5$ mm and decreases slightly at $t_0 = 3.0$ mm. The evolution is somewhat different for Fe30Mn, with a peak value of w_e at $t_0 = 2.0$ mm and with w_e decreasing more than in Fe26Mn above the peak thickness. On the contrary to the large difference in W_f^{uni} (Figure 1), the values of w_e of Fe26Mn overlap with DP-36%. The w_e of Fe30Mn is slightly higher than Fe26Mn for $t_0 \geq 1.0$ mm, but is lower at $t_0 = 0.6$ mm. A linear regression of w_e with t_0 is performed to separate Γ_0 and βw_n, as shown in Table 2. The contribution of Γ_0 in Fe26Mn is higher than in Fe30Mn, while βw_n of Fe26Mn is smaller. This indicates that Fe26Mn involves more energy dissipation in the damage and fracture processes, which is thickness independent; while higher crack tip necking energy is dissipated in the Fe30Mn, with a fracture resistance much more sensitive to thickness. To a first approximation, the thickness at peak w_e (noted as t_{peak}) should scale with the plane-stress plastic zone size (r_p) [32], which is equal to

$$r_p \approx \frac{1}{3}\frac{E\Gamma_0}{\sigma_0^2}, \tag{5}$$

where E is the Young's modulus, σ_0 is the yield strength and Γ_0 is taken as the plane-stress critical energy release

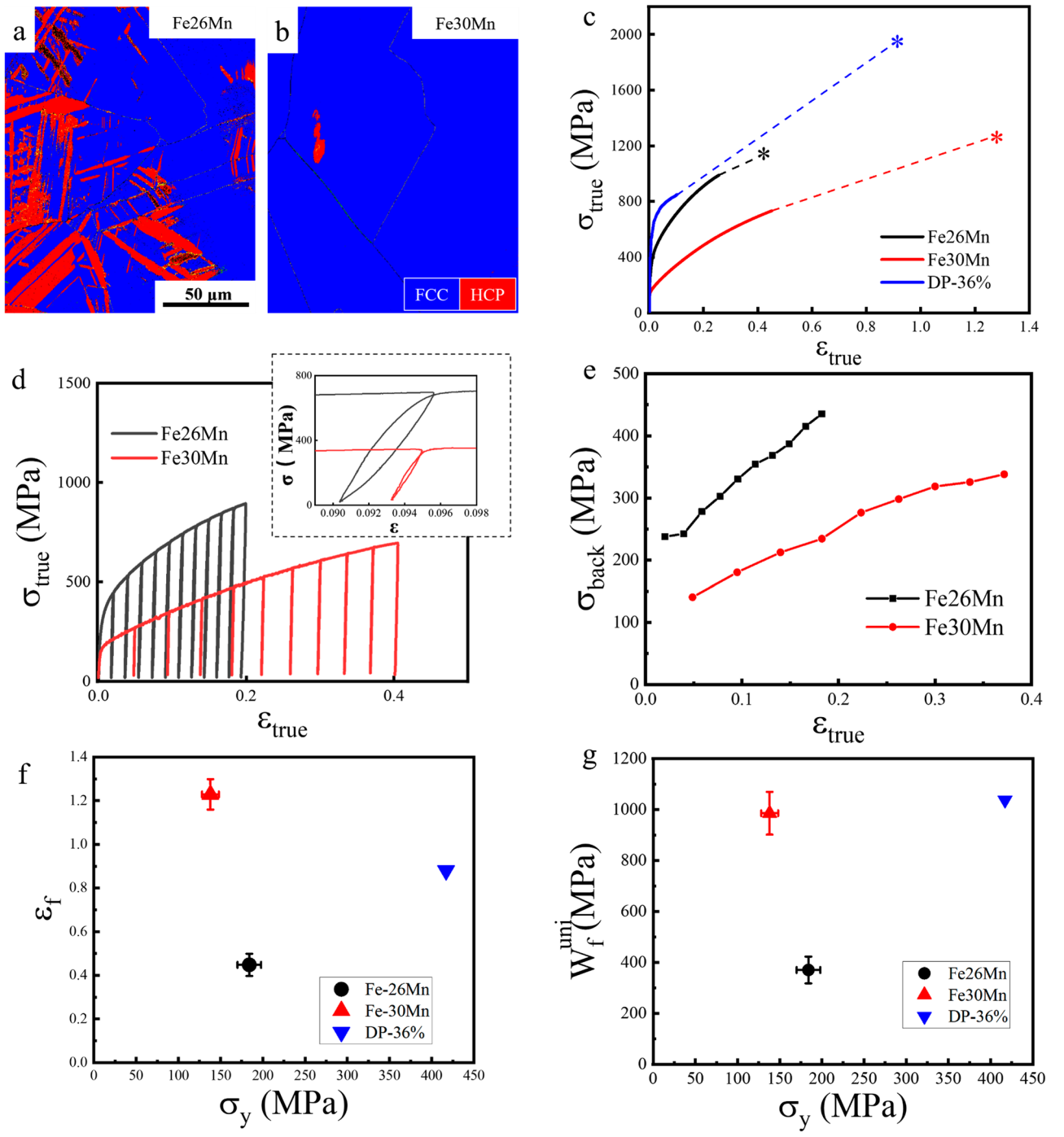

Figure 1. Microstructures and uniaxial tension response of the FeMn alloys; (a) and (b) microstructures of Fe26Mn and Fe30Mn alloys characterized by EBSD with the same scale bar for both micrographs; (c) true stress-true strain responses with the approximated extension to fracture; (d) the results of the LUR experiments associated with the typical hysteresis during the unloading-reloading cycle; (e) the measurement of the back stress; (f) and (g) materials property maps in terms of ε_f-σ_y and W_f^{uni}-σ_y, respectively.

Table 1. Parameters entering the EWF analysis and linear regression.

	t_o (mm)	w_e (J/mm^2)	αw_p(J/mm^3)	R^2		t_o (mm)	w_e(J/mm^2)	αw_p(J/mm^3)	R^2
Fe26Mn	0.6	0.196	0.023	0.88	Fe30Mn	0.6	0.157	0.038	0.94
	1	0.244	0.023	0.98		1	0.324	0.047	0.94
	1.4	0.241	0.028	0.91		1.4	0.295	0.058	0.99
	2	0.384	0.021	0.75		2	0.485	0.058	0.85
	2.5	0.419	0.017	0.92		2.5	0.468	0.076	0.86
	3	0.404	0.027	0.89		3	0.437	0.070	0.99

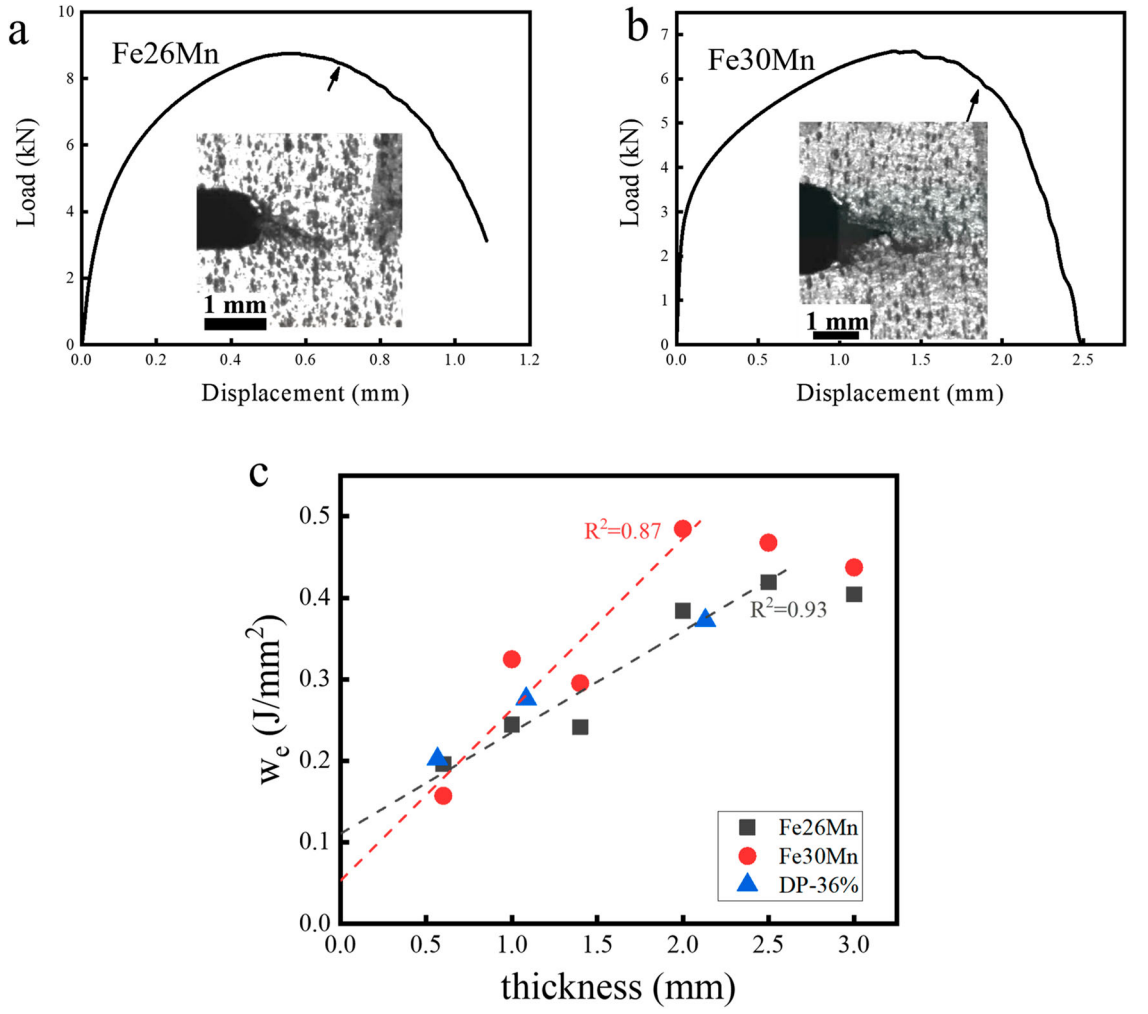

Figure 2. Results of the EWF measurements; (a) and (b) typical load-displacement curve of Fe26Mn and Fe30Mn alloys, respectively; (c) variation of EWF with thickness of the three steels.

Table 2. Partitioning of the work of necking w_n and work of fracture Γ_0.

	Γ_0 (J/mm^2)	βw_n (J/mm^3)	R^2	σ_0 (MPa)	$\varepsilon_f\|_{plane\ strain}$	n
Fe26Mn	0.110	0.124	0.93	184	0.29	0.23
Fe30Mn	0.053	0.210	0.87	138	0.66	0.40
DP-36%	0.137	0.115				

rate [15]. Therefore, the following dimensional relationship should be respected

$$\frac{t_{peak}^{Fe30Mn}}{t_{peak}^{Fe26Mn}} = \frac{\Gamma_0^{Fe30Mn}}{\Gamma_0^{Fe26Mn}} \frac{\sigma_0^2|_{Fe26Mn}}{\sigma_0^2|_{Fe30Mn}} \tag{6}$$

The estimated ratio $\frac{t_{peak}^{Fe30Mn}}{t_{peak}^{Fe26Mn}}$ in Equation (6) is equal to 0.86, in good agreement with the experimental value (2.0/2.5 = 0.8). Notice that the precise relationship between t_{peak} and r_p is still a matter of open debate in the literature [17,38].

Macro- and microscopic characterizations of the fracture surfaces of the broken DENT specimens are shown in Figure 3. Both materials present a progressive development of the neck. The equivalent fracture strain ($\varepsilon_f^{eq}|_{plane\ strain}$) is given by

$$\varepsilon_f^{eq}|_{plane\ strain} = \frac{2}{\sqrt{3}} \ln\left(\frac{t_0}{t_f}\right), \tag{7}$$

where t_f is the thickness corresponding to the fracture surface, assuming plane strain in the ligament direction. The equivalent fracture strain in the steady state regime is equal to 0.29 and 0.66 for Fe26Mn and Fe30Mn, respectively. But the two alloys present very different microscopic features. As shown in Figure 3(c), the fracture surface of Fe26Mn is covered both by planar facets and by dimples. The planar facets most probably result from

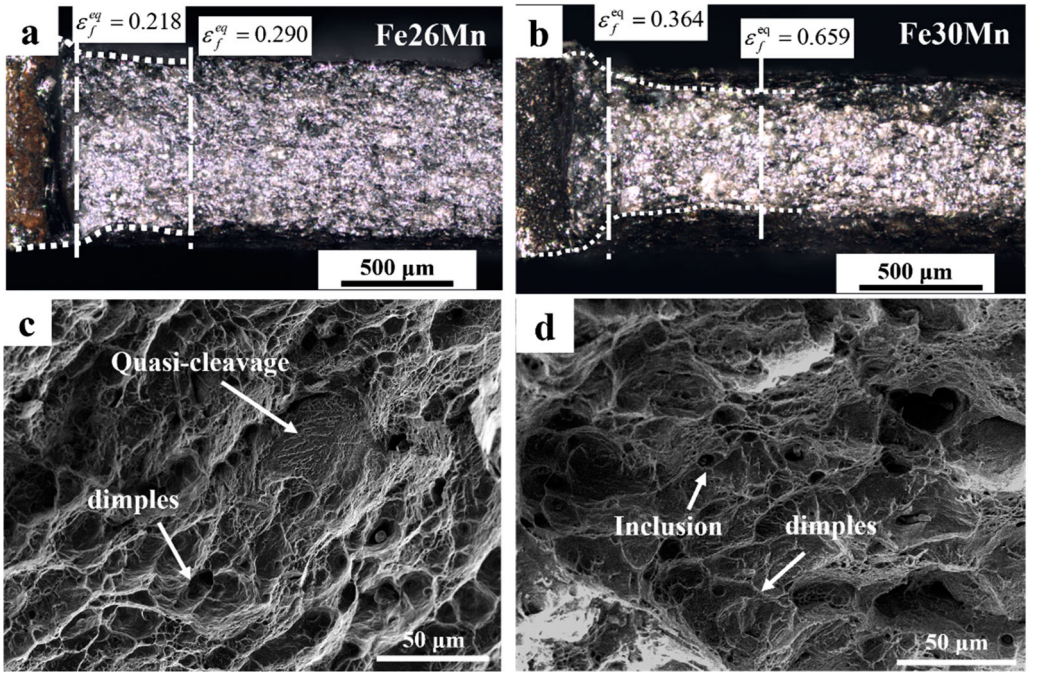

Figure 3. Micrographs of the fracture surfaces of the broken DENT specimens; (a) and (b) optical micrographs of Fe26Mn and Fe30Mn; (c) and (d) SEM micrographs of Fe26Mn and Fe30Mn.

the quasi-cleavage induced by the ε-martensite [5,6]. The Fe30Mn involves only dimples, and the larger dimples are linked by a second population of smaller voids (Figure 3(d)). Inclusions were occasionally observed at the bottom of the large dimples.

A DENT test has been interrupted just after cracking initiation, and characterizations were performed in the near crack tip region along the mid-thickness section. For Fe26Mn, the crack propagates in a continuous manner, and crack deflection occurs as a result of the branching process (Figure 4(a)). The EBSD phase map shows that crack branching occurs in a region dominated by the ε-martensite, and sharp microcracks get arrested by the surrounding austenite (Figure 4(b)). The distribution of KAM indicates that intensive plastic deformation occurs in both the ε-martensite and austenite, which suggests significant plastic co-deformation (Figure 4(c)). The Fe30Mn alloy demonstrates a different cracking mechanism. The main crack extends by joining the cavities in the near crack tip region. Figure 4(d) shows two kinds of damage features, including a void after substantial growth (to a size of $\sim$20 µm) and a sharp microcrack. The EBSD phase map in Figure 4(e) shows that the void was formed in the austenite, while the microcrack is formed in the ε-martensite, which is arrested by the austenite. The distribution of KAM in Figure 4(f) also gives evidences of the plastic co-deformation of ε-martensite and austenite in the Fe30Mn. Note that twin boundaries can be found in the austenite in Fe30Mn at the near crack tip region, but deformation twinning is not obvious in Fe26Mn, as shown in Figure S5. The correlation between twinning and damage formation is not obvious according to the observations.

Discussion

The EWF indicates a different ranking of the fracture properties when comparing with uniaxial tension in terms of ε_f and W_f^{uni}, respectively. The Fe30Mn shows a slightly larger EWF than Fe26Mn down to $t_0 = 1.0$ mm, but the ranking is inverted at lower thickness. In addition, the fracture resistance of Fe26Mn is at the level of DP-36% in this range of thickness. These results are somewhat not consistent with the general impression that ε-martensite deteriorates the fracture resistance. It has been reported that the HCP structure of ε-martensite involves less than 5 independent slip systems, and the stress concentration along ε-martensite/ε-martensite or along ε-martensite/grain boundaries interfaces could induce premature failure [5,6,39]. Therefore, the interpretation of the previous measurements of fracture resistance should be developed based on a deeper understanding of the failure process of the DENT specimens and of the two contributions entering EWF.

During DENT testing, ε-martensitic transformation occurs during the diffuse (and thus relatively small levels of) plastic deformation inside the ligament before cracking and, thereafter, is amplified more locally in the

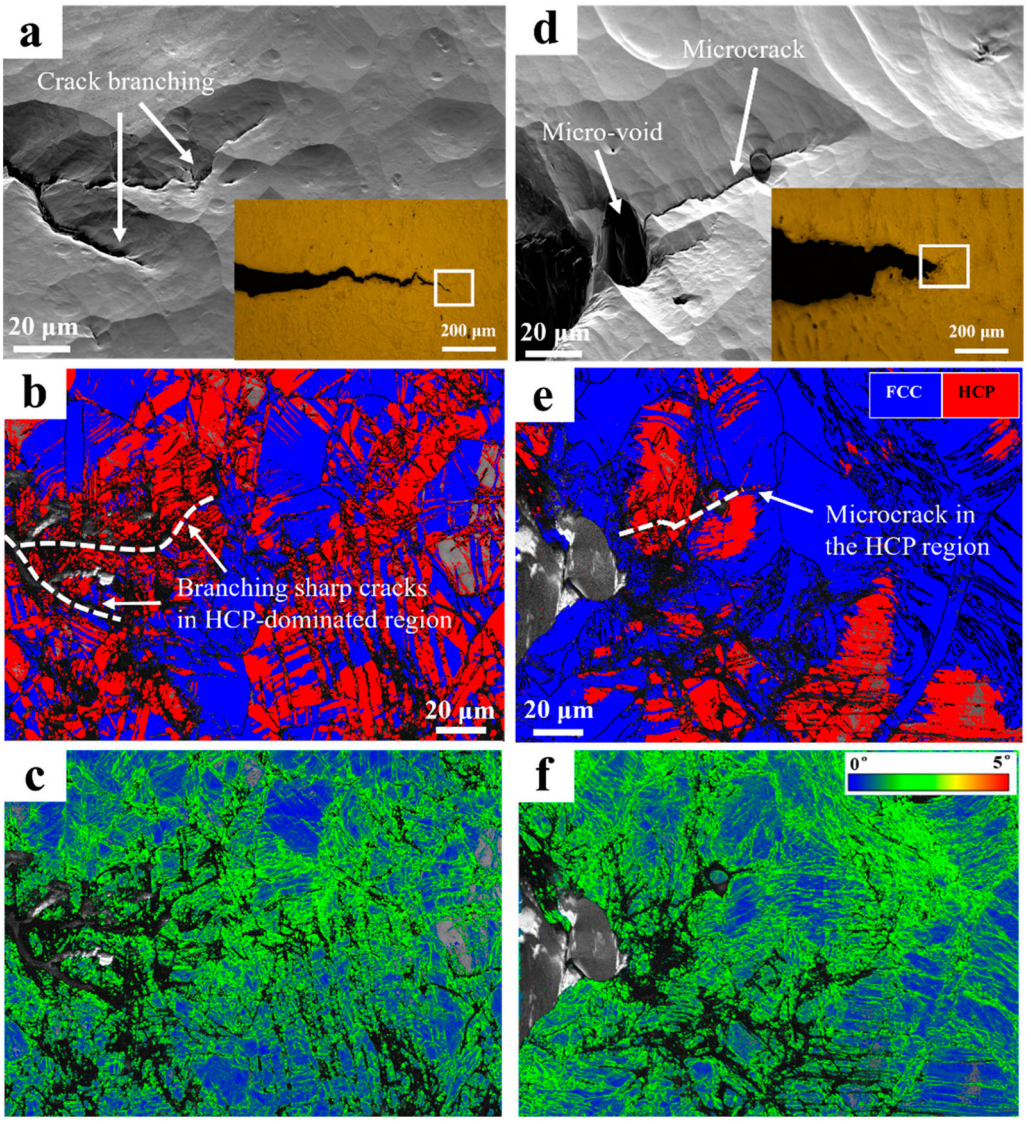

Figure 4. Microstructure characterization of the crack tip region; (a) micrograph showing the crack morphology in Fe26Mn; (b) and (c) phase map and distribution of KAM determined by EBSD; (d) micrograph of the crack morphology in Fe30Mn; (e) and (f) phase map and distribution of KAM determined by EBSD.

FPZ during cracking. This can be substantiated by the results of Figure 4 that the microstructures at the near crack tip region are significantly changed from the initial state. The TRIP effect could enhance the strain hardening capacity locally and thus the flow stress level. In addition, the occurrence of ε-martensitic transformation results in that the DENT tests are actually probing the fracture resistance of a transformed material, as the FPZ contains essentially transformed material, which is a key point in the interpretation of the measurements. This has been already explained for multiphase TRIP-assisted steels in the past [19,40]. In this work, the comparison between Fe26Mn and Fe30Mn involves a difference in the initial ε-martensite fraction and also a difference in the transformation kinetics due to different austenite stability. Thus, the comparison could clearly reveal the overall effect of ε-martensite on the fracture resistance, when the sources of energy dissipations in the FPZ can be separated, e.g. by applying the EWF concept.

The values of EWF, defined as the fracture resistance of ductile sheet materials, can be partitioned into the work for material separation and the work for cracking tip necking. By applying equation (4), for $t_0 = 1.4$ mm, the ratio of Γ_0/Γ_n is 0.63 for Fe26Mn and 0.18 for Fe30Mn, and the higher fracture resistance of Fe30Mn is attributed to the larger work of necking; while for $t_0 = 0.6$ mm, the Γ_0/Γ_n is 1.49 for Fe26Mn and is 0.42 for Fe30Mn. This means that, when the contribution of necking work is limited by the small thickness, it is the higher contribution of Γ_0 that contributes to a higher fracture

resistance of Fe26Mn. The term Γ_0 primarily scales with $\sigma_0 X_0$ [41], with X_0 the mean distance between dimples. X_0 was found equal to 4.14 ± 2.96 µm for Fe30Mn and 3.13 ± 1.88 µm for Fe26Mn, and the more ε-martensite formation in Fe26Mn during the failure of DENT specimens is actually not reducing the void spacing. Hence, it is the higher strength that explains the higher Γ_0 for Fe26Mn. According to the observations in Figure 4, the microcracks formed in ε-martensite get blunted by the surrounding austenite. And the crack branching behavior in Fe26Mn could also contribute to enhancing the energy dissipation by generating two active FPZ, and to releasing the local stress concentration through mutual crack tip shielding. In addition, the ε-martensite, as a distributed second phase instead of a bulk material, can undergo appreciable plastic strain before nucleating a microcrack, as indicated by the accumulation of KAM. These micromechanisms favor an increase of the cracking resistance, and provide, from a microstructrual viewpoint, an explanation why more ε-martensite formation in Fe26Mn does not reduce the work of fracture. As for the larger βw_n value of Fe30Mn than of Fe26Mn, it can be rationalized by both the larger equivalent fracture strain and the larger size of the necking zone due to a higher strain hardening coefficient [17,18].

Conclusions

In summary, this study delivers original results about the fracture resistance of high-Mn steels involving ε-martensite formation. Under uniaxial tension, the presence of ε-martensite obviously deteriorates the tensile elongation. But when considering the cracking resistance from a sharp defect, the EWF measurements show a different ranking of fracture resistance. The Fe26Mn with more significant ε-martensite formation presents a slightly lower w_e than Fe30Mn at $t_0 > 1.0$ mm, and the ranking is inverted at a smaller thickness. The higher w_e of Fe30Mn at a larger thickness is due to the contribution of crack tip necking work, while the higher w_e of Fe26Mn at a smaller thickness is due to the larger work for material separation. The measurement of the work for material separation is interpreted based on the observations of the substantial plastic co-deformation of ε-martensite with austenite, the blunting and branching of microcracks and that more ε-martensite is not reducing the void spacing.

Disclosure statement

No potential conflict of interest was reported by the author(s).

Funding

This study is supported by the National Key Research and Development Program of China [grant number 2023YFB3712703] and National Natural Science Foundation of China [grant numbers 51927801, 52001166, 92263201].

ORCID

Pascal Jacques http://orcid.org/0000-0002-2814-4060

References

[1] Bouaziz O, Allain S, Scott CP, et al. High manganese austenitic twinning induced plasticity steels: a review of the microstructure properties relationships. Curr Opin Solid State Mater Sci. 2011;15:141–168.
[2] De Cooman BC, Estrin Y, Kim SK. Twinning-induced plasticity (TWIP) steels. Acta Mater. 2018;142:283–362. doi:10.1016/j.actamat.2017.06.046
[3] Frommeyer G, Brüx U, Neumann P. Supra-ductile and high-strength manganese-TRIP/TWIP steels for high energy absorption purposes. ISIJ Int. 2003;43:438–446. doi:10.2355/isijinternational.43.438
[4] Fang X, Xue Q, Yu K, et al. Superior strength-ductility synergy by hetero-structuring high manganese steel. Mater Res Lett. 2020;8:417–423. doi:10.1080/21663831.2020.1780330
[5] Koyama M, Sawaguchi T, Tsuzaki K. Premature fracture mechanism in an Fe-Mn-C austenitic steel. Metall Mater Transact A. 2012;43:4063–4074. doi:10.1007/s11661-012-1220-7
[6] Koyama M, Kaneko T, Sawaguchi T, et al. Microstructural damage evolution and arrest in binary Fe-high-Mn alloys with different deformation temperatures. Int J Fracture. 2018;213:193–206. doi:10.1007/s10704-018-0307-6
[7] Koyama M, Lee T, Lee CS, et al. Grain refinement effect on cryogenic tensile ductility in a Fe-Mn-C twinning-induced plasticity steel. Mater Des. 2013;49:234–241. doi:10.1016/j.matdes.2013.01.061
[8] Choi JH, Jo MC, Lee H, et al. Cu addition effects on TRIP to TWIP transition and tensile property improvement of ultra-high-strength austenitic high-Mn steels. Acta Mater. 2019;166:246–260. doi:10.1016/j.actamat.2018.12.044
[9] Koyama M, Sawaguchi T, Tsuzaki K. TWIP effect and plastic instability condition in an Fe-Mn-C austenitic steel. ISIJ Int. 2013;53:323–329. doi:10.2355/isijinternational.53.323
[10] Pineau A, Benzerga AA, Pardoen T. Failure of metals I: brittle and ductile fracture. Acta Mater. 2016;107:424–483. doi:10.1016/j.actamat.2015.12.034
[11] Antolovich SD, Armstrong RW. Plastic strain localization in metals: origins and consequences. Prog Mater Sci. 2014;59:1–160. doi:10.1016/j.pmatsci.2013.06.001
[12] Xiong Z, Jacques PJ, Perlade A, et al. Characterization and control of the compromise between tensile properties and fracture toughness in a quenched and partitioned steel. Metall Mater Transact A. 2019;50:3502–3513. doi:10.1007/s11661-019-05265-2

[13] Xiong Z, Jacques PJ, Perlade A, et al. Ductile and intergranular brittle fracture in a two-step quenching and partitioning steel. Scr Mater. 2018;157:6–9. doi:10.1016/j.scriptamat.2018.07.030
[14] Lai Q, Chen Z, Wei Y, et al. Towards the understanding of fracture resistance of an ultrahigh-strength martensitic press-hardened steel. J Mater Res Technol. 2023;27:1996–2006. doi:10.1016/j.jmrt.2023.10.090
[15] Pardoen T, Marchal Y, Delannay F. Thickness dependence of cracking resistance in thin aluminium plates. J Mech Phys Solids. 1999;47:2093–2123. doi:10.1016/S0022-5096(99)00011-3
[16] Kaneko T, Koyama M, Fujisawa T, et al. Combined multi-scale analyses on strain/damage/microstructure in steel: example of damage evolution associated with ε-martensitic transformation. ISIJ Int. 2016;56:2037–2046. doi:10.2355/isijinternational.ISIJINT-2016-272
[17] Pardoen T, Hachez F, Marchioni B, et al. Mode I fracture of sheet metal. J Mech Phys Solids. 2004;52:423–452. doi:10.1016/S0022-5096(03)00087-5
[18] Hilhorst A, Jacques PJ, Pardoen T. Towards the best strength, ductility, and toughness combination: high entropy alloys are excellent, stainless steels are exceptional. Acta Mater. 2023;260:119280. doi:10.1016/j.actamat.2023.119280
[19] Lacroix G, Pardoen T, Jacques PJ. The fracture toughness of TRIP-assisted multiphase steels. Acta Mater. 2008;56:3900–3913. doi:10.1016/j.actamat.2008.04.035
[20] Cotterell B, Reddel JK. The essential work of plane stress ductile fracture. Int J Fract. 1977;13(3):267–277. doi:10.1007/BF00040143
[21] Mai YW. On the plane-stress essential fracture work in plastic failure of ductile materials. Int J Mech Sci. 1993;35:995–1005. doi:10.1016/0020-7403(93)90051-U
[22] Pardoen T, Marchal Y, Delannay F. Essential work of fracture compared to fracture mechanics – towards a thickness independent plane stress toughness. Eng Fract Mech. 2002;69:617–631. doi:10.1016/S0013-7944(01)00099-6
[23] Ismail K, Perlade A, Jacques PJ, et al. Outstanding cracking resistance of fibrous dual phase steels. Acta Mater. 2021;207:116700. doi:10.1016/j.actamat.2021.116700
[24] Schuman VH. Martensitische Umwandlung in austenitischen Mangan-Kohlenstoff-Stählen. Neue Hütte. 1972;17:605–609.
[25] Liang X, McDermid JR, Bouaziz O, et al. Microstructural evolution and strain hardening of Fe-24Mn and Fe-30Mn alloys during tensile deformation. Acta Mater. 2009;57:3978–3988. doi:10.1016/j.actamat.2009.05.003
[26] Nakano J, Jacques PJ. Effects of the thermodynamic parameters of the hcp phase on the stacking fault energy calculations in the Fe-Mn and Fe-Mn-C systems. CALPHAD. 2010;34:167–175. doi:10.1016/j.calphad.2010.02.001
[27] Sohrabi MJ, Naghizadeh M, Mirzadeh H. Deformation-induced martensite in austenitic stainless steels: a review. Arch Civil Mech Eng. 2020;20:124. doi:10.1007/s43452-020-00130-1
[28] Lai Q, Yang H, Wei Y, et al. Transformation plasticity in high strength, ductile ultrafine-grained FeMn alloy processed by heavy ausforming. Int J Plast. 2022;148:103151. doi:10.1016/j.ijplas.2021.103151
[29] Choisez L, Ding L, Marteleur M, et al. High temperature rise dominated cracking mechanisms in ultra-ductile and tough titanium alloy. Nat Commun. 2020;11:2110. doi:10.1038/s41467-020-15772-1
[30] Yang M, Pan Y, Yuan F, et al. Back stress strengthening and strain hardening in gradient structure. Mater Res Lett. 2016;4:145–151. doi:10.1080/21663831.2016.1153004
[31] Zhu Y, Ameyama K, Anderson PM, et al. Heterostructured materials: superior properties from hetero-zone interaction. Mater Res Lett. 2021;9:1–31. doi:10.1080/21663831.2020.1796836
[32] Zhu Y, Wu X. Heterostructured materials. Prog Mater Sci. 2023;131:101019. doi:10.1016/j.pmatsci.2022.101019
[33] Chen J, Ren J, Liu Z, et al. Interpretation of significant decrease in cryogenic-temperature Charpy impact toughness in a high manganese steel. Mater Sci Eng A. 2018;737:158–165.
[34] Sohn SS, Hong S, Lee J, et al. Effects of Mn and Al contents on cryogenic-temperature tensile and Charpy impact properties in four austenitic high-Mn steels. Acta Mater. 2015;100:39–52. doi:10.1016/j.actamat.2015.08.027
[35] Yoo MH, Morris JR, Ho KM, et al. Nonbasal deformation modes of HCP metals and alloys: role of dislocation source and mobility. Metall Mater Transact A. 2002;33:813–822.
[36] Clutton, E, Essential work of fracture. In Moore DR, Pavan A, Williams JG, editors. European structural integrity society. Oxford: Elsevier; 2001. p. 177–195.
[37] Hilhorst A, Pardoen T, Jacques PJ. Optimization of the essential work of fracture method for characterization of the fracture resistance of metallic sheets. Eng Fract Mech. 2022;268:108442. doi:10.1016/j.engfracmech.2022.108442
[38] Broek D. Elementary engineering fracture mechanics. 4th ed. Hague: Martinus Nijhoff Publishers; 1991.
[39] Wei S, Kim J, Tasan CC. Boundary micro-cracking in metastable Fe45Mn35Co10Cr10 high-entropy alloys. Acta Mater. 2019;168:76–86. doi:10.1016/j.actamat.2019.01.036
[40] Jacques P, Furnémont Q, Pardoen T, et al. On the role of martensitic transformation on damage and cracking resistance in trip-assisted multiphase steels. Acta Mater. 2001;49:139–152. doi:10.1016/S1359-6454(00)00215-9
[41] Pardoen T, Hutchinson JW. Micromechanics-based model for trends in toughness of ductile metals. Acta Mater. 2003;51:133–148. doi:10.1016/S1359-6454(02)00386-5